

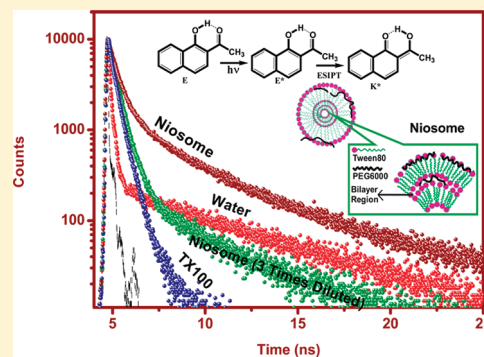
# Photophysics and Photodynamics of 1'-Hydroxy-2'-acetonaphthone (HAN) in Micelles and Nonionic Surfactants Forming Vesicles: A Comparative Study of Different Microenvironments of Surfactant Assemblies

Sarthak Mandal, Vishal Govind Rao, Chiranjib Ghatak, Rajib Pramanik, Souravi Sarkar, and Nilmoni Sarkar\*

Department of Chemistry, Indian Institute of Technology, Kharagpur, West Bengal 721302, India

Supporting Information

**ABSTRACT:** The effect of different microenvironments inside various biomimicking supramolecular assemblies of ionic (SDS/CTAB) and nonionic (TX100) micelles and nonionic surfactants (Tween-80/PEG-6000) forming vesicles (niosome) on the photophysical and rotational dynamical properties of 1'-hydroxy-2'-acetonaphthone (HAN) have been studied using steady-state and time-resolved fluorescence spectroscopy. Enhanced fluorescence intensity with a significant blue shift and longer emission lifetime of the caged tautomers of HAN indicate modulation of photophysics of HAN upon encapsulation in both micellar assemblies and the niosome system. The binding constant and free energy change for the complexation of HAN with micelles and niosome demonstrate a comparative study on the binding efficiency of the different assemblies depending on the nature of microenvironments toward HAN. The enhancement in the steady-state anisotropy in niosome solutions compared with that in pure aqueous solution indicates that HAN is located inside the motionally restricted bilayer region of niosome. The fluorescence quenching experiment further reveals the probable location of HAN in micelles and niosome. In TX100 micelles, the obtained lifetime values are 417 ps and 1.63 ns for the caged tautomers, whereas in the comparatively more rigid and confined environment provided by niosome those values are 444 ps and 2.5 ns. The rotational relaxation time constants for the caged tautomers in niosome are also found to be higher than those in micelles. The observed difference in binding ability of the different assemblies is due to the difference in the extent of water penetration and different extent of rigidity around the fluorophore.



## 1. INTRODUCTION

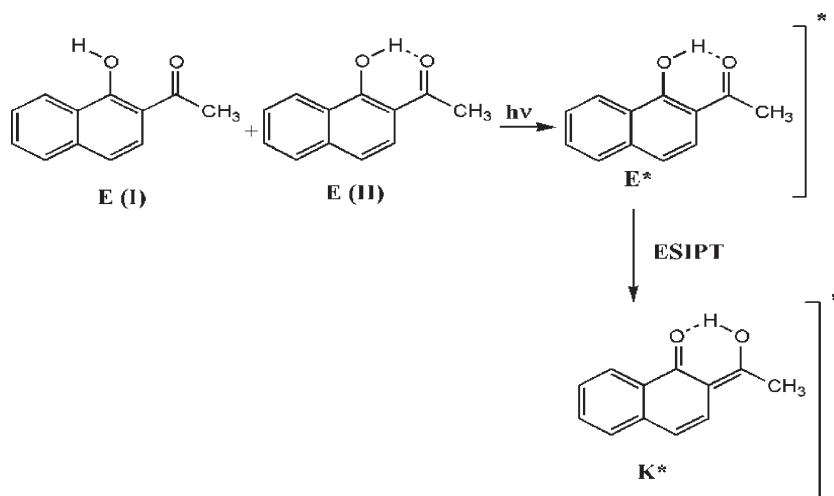
In recent years, there has been an increasing interest in studying excited-state proton transfer (ESPT) dynamics in different self-organized supramolecular assemblies like cyclodextrins,<sup>1–8</sup> microemulsions,<sup>9,10</sup> micelles,<sup>11–14</sup> reverse micelles,<sup>15–17</sup> mixed micelles,<sup>18,19</sup> vesicles,<sup>20,21</sup> and so on. Basically, interest in such systems originates from a broad range of applications and also because of their unique ability to mimic many complex biological systems in a much simpler form.<sup>22,23</sup> Surfactant molecules, the common and useful<sup>24</sup> amphiphilic molecules, self-assembled into a variety of organized assemblies depending on their structures, concentrations, compositions, solubilizing media, and the method used to prepare them.<sup>25</sup> While micelles are common surfactant aggregates, vesicles can be prepared from phospholipid, nonionic surfactant, and mixed cationic and anionic surfactant molecules under certain concentrations and compositions. Vesicles formed from nonionic surfactants are known as niosomes and vesicles that are comprised of phospholipids are called liposomes. Both niosomes and liposomes are similar in structure and properties. Recently, Liu and Guo et al.<sup>26–28</sup> have synthesized highly stable niosomes in aqueous medium using Tween-80 as nonionic surfactant and PEG-6000 as additive by a simple

sonication method. They have also shown that niosomes have strong hydrotrope solubilizing action; that is, they can carry both hydrophobic and hydrophilic drug molecules through encapsulation.<sup>26,28</sup> The bilayer of vesicles is mainly comprised of the head groups of amphiphiles and a small part of water remains within that. The water molecules present in the hydration layer of micelles and vesicles play a crucial role in the photophysical and photodynamical behavior of a confined spectroscopic probe.<sup>29,30</sup> Recently, Tahara et al.<sup>31</sup> have studied the structure and orientation of the water molecules at charged lipid–water interfaces. The importance of both micelles and niosomes lies in the fact that these are extensively used as a potential drug delivery system.<sup>32–35</sup> The relatively low cost of surfactant molecules over lipid molecules for the preparation of vesicles has made niosomes an active topic of research in recent years. Moreover, the simpler method for the preparation of niosomes over liposomes helps greatly in chemical and biological applications, as well as in industrial applications.<sup>35</sup>

**Received:** May 6, 2011

**Revised:** September 2, 2011

**Published:** September 09, 2011

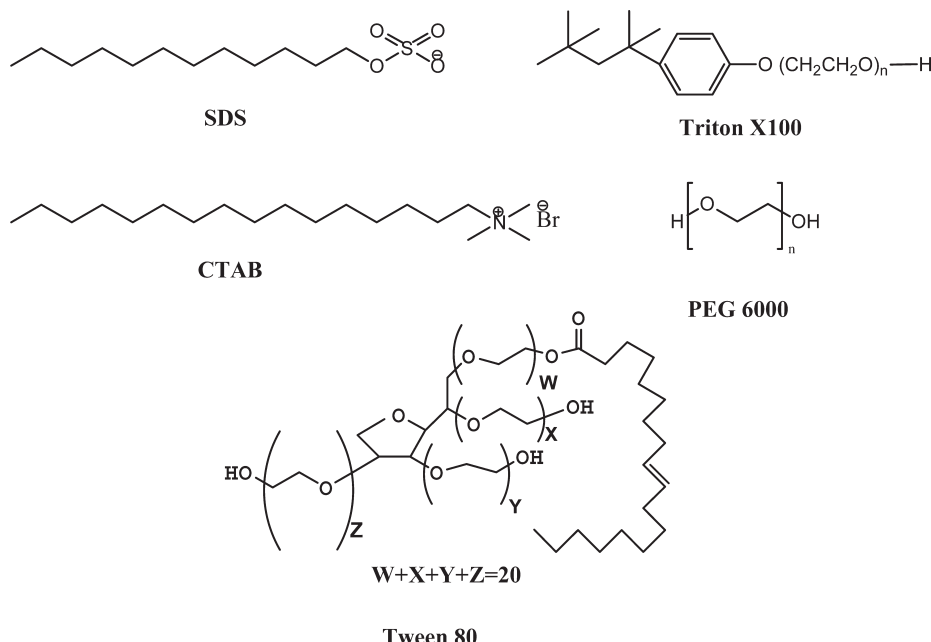
**Scheme 1.** Schematic Representation of the Different Tautomers of HAN Involved in the ESIPT Process

In 1956, Weller first observed excited-state intramolecular proton transfer (ESIPT) in methyl salicylate (MS).<sup>36,37</sup> Since then, though many works have been performed on proton transfer (PT) processes using various proton transfer probes<sup>38–50</sup> in the last few decades, but studies on the photophysical behavior of 1'-hydroxy-2'-acetonaphthone (HAN), which has potential ability in polymer protection,<sup>51</sup> are limited. Furthermore, the application of ESIPT reactions for the development of white-light-emitting diodes, photostabilizers, proton transfer lasers, etc. also makes it more interesting to study.<sup>52–55</sup>

1'-Hydroxy-2'-acetonaphthone (HAN) is such an intramolecular proton transfer probe, which is reported to be planar with a strong intramolecular hydrogen bond in its ground-state enol conformer (E).<sup>56</sup> This probe molecule upon photoexcitation undergoes a rapid ESIPT reaction, which leads to the formation of a keto type tautomer (K\*) as shown in Scheme 1. In 1993, Douhal et al.<sup>57</sup> observed dual fluorescence of HAN under free jet expansion conditions. They concluded that this dual nature of the dispersed emission spectrum originates due to an ESIPT process where the short and long wavelength emissions are attributed to the enol form (E\*) and keto (K\*) form, respectively. After that, many theoretical studies<sup>56,58,59</sup> supported by experimental observations<sup>60–63</sup> established the involvement of PT processes in the excited state of HAN. The Cheng group<sup>62</sup> using a femtosecond experiment observed that ESIPT of HAN occurs on the picosecond time scale. Later on, femtosecond pump–probe experiments performed by Lochbrunner et al.<sup>63</sup> showed that it happens within 30 fs. Tobita et al.<sup>65</sup> studied the proton transfer of HAN and its related compounds like HNA (1-hydroxy-2-naphthaldehyde) and HMN (methyl-1-hydroxy-2-naphthoate) using laser photolysis and a time-resolved thermal lensing technique. They found an ESIPT reaction in HAN and HNA but not in HMN. However, Catalan et al.<sup>66–68</sup> did not recognize the ESIPT reaction in HAN. So far, Douhal et al.<sup>56,58,64</sup> reported that the proton-transferred keto tautomer (K\*) may subsequently form a rotamer (which they assigned as KR\*) through the twisting motion of C–C bond between the newly protonated acetyl group and naphthalene moiety. Moreover, this rotamer is reported to be more stable than the keto form, but recently, Moreno and Luch et al.<sup>59</sup> on the basis of their improved level of theoretical calculations concluded that KR\* structures are found at higher energies (11.10 kcal mol<sup>-1</sup> above E\*). Very recently, Catalan et al.<sup>69</sup> discard

the existence of KR\* because they did not find any energy minimum for KR\* at the TDDFT level; rather they found a new structure (which they assigned as KROH), having an energy minimum in the ground state. However, it is very true that all theoretical calculations based on simple techniques and calculations are mostly for gas phase and suitable for ground state and hence cannot be taken as a strong basis to explain the photophysics of HAN in solutions where there are many other factors like polarity, H-bonding ability, viscosity, etc. to take into account. This fact has already been reflected in the different theoretical results obtained for KR\* by different groups using different methods. Therefore, much more accurate methods are necessary as indicated by Douhal et al.<sup>64</sup> and Ortiz-Sánchez et al.<sup>59</sup> to actually ascertain the relative position of KR\* with respect to E\* and K\* and to explain the role of KR\* in the photophysics of HAN. Catalan et al.<sup>69</sup> proposed that the ground-state enol form of HAN upon photoexcitation produces two enol forms of similar energies. One is a stable enol form that emits through the minimum in the S<sub>0</sub> state and produces another new enol form, which is also emissive. This new enol form where the methyl group is staggered with the carbonyl oxygen in the excited state may result in the keto form or KROH after an ultrafast proton transfer process. Many other groups have reported that the fluorescence emission of HAN in aprotic solvents originates from the keto form.<sup>59,72</sup> Still there is some controversy whether the emission results from the enol form or from the proton-transferred keto tautomer. Ortiz-Sánchez et al. proposed that emission of HAN may result from relaxation of both E\* and K\* assuming that they are in equilibrium because of a very small potential energy barrier. However, the emission from the proton-transferred keto tautomer has been supported by previously reported results for the ESIPT of HNA, a structural analogue of HAN,<sup>20,21,70</sup> and here it is important to note that the spectral properties of HNA are similar to that of HAN.

The photodynamics of HAN has been studied in different homogeneous solvents to see the effect of temperature, viscosity, H-bonding ability, and polarity of the solvents.<sup>71</sup> In neat non-polar solvents like cyclohexane and methylcyclohexane, a broad emission spectrum with the maximum centered at 480 nm and a shoulder at 450 nm is observed at room temperature.<sup>2,72</sup> The excitation spectra of HAN in cyclohexane monitored at the emission wavelengths of 450 and 480 nm are also found to be well-correlated with the absorption spectra of HAN. Moreover, Catalan et al.<sup>69</sup> experimentally have observed that on lowering the temperature the absorption band exhibits the same vibronic structure

**Scheme 2.** Structures of Surfactants Used for the Preparation of Different Supramolecular Assemblies

as the emission band. Therefore, the emitting molecular structure is very similar to the absorbing structure. In neutral water, the maximum of the fluorescence emission spectrum of HAN appears at 490 nm. Catalan et al.<sup>67</sup> observed that the larger the polarity of the solvent the larger is the red shift in the emission spectra of HAN. In a series of papers,<sup>73–76</sup> the Douhal group have described the photophysical behavior of HAN confined in different supramolecular assemblies of cyclodextrins. Very recently, studies have been performed in the restricted microenvironment of human serum albumin (HSA) and modified cyclodextrins.<sup>76</sup> In these reports, enhancement of fluorescence intensity along with a significant blue shift of the emission maxima (except in  $\gamma$  CD) are observed. This altered photophysics is due to the formation of inclusion complexes of HAN with various cyclodextrins and in the hydrophobic pocket of HSA in different ways depending upon the size of the nanocavity. For example, the stoichiometric ratio of inclusion complexes (HAN/CD) formed by  $\beta$  and  $\gamma$  cyclodextrins is 1:1, whereas that for  $\alpha$  cyclodextrins that is 1:2. Surfactant aggregates like micelles and niosomes are very useful for examining the effect of binding of a spectroscopic probe.<sup>26–28,77–79</sup> However, there is no such study on varying nature of microenvironments formed by the self-aggregation of the different types of surfactant molecules. So, in this work, the study of photophysical behavior of HAN confined in different micelles formed by surfactants like cetyltrimethylammonium bromide (CTAB), Triton X-100, and sodium dodecyl sulfate (SDS) and also in a nonionic surfactant like Tween-80 and PEG-6000, forming vesicles (niosomes) has been investigated. We have also investigated the binding ability of the different supramolecular assemblies having different microenvironments around the fluorophore. Finally, we have shown that the more rigid and confined environment inside the niosome is a better model for studying the binding of a spectroscopic probe like HAN.

## 2. EXPERIMENTAL SECTION

**2.1. Chemicals.** 1'-Hydroxy-2'-acetonaphthone (HAN) was taken from Sigma Aldrich and used as received. The anionic

surfactant sodium dodecyl sulfate (SDS), the cationic surfactant cetyltrimethylammonium bromide (CTAB), and the neutral surfactant reduced Triton X-100 (TX-100) were purchased from Sigma Aldrich and used as received to prepare micelles. For the preparation of niosomes, we used nonionic surfactants Tween-80 and PEG-6000, which were also taken from Sigma Aldrich. The structures of all the chemicals used in this experiment are given in Scheme 2.

**2.2. Instruments and Methods.** Steady-state absorption and emission spectra were recorded on a Shimadzu (model UV 1601) UV-vis spectrophotometer and an Hitachi (model no. F-7000) spectrofluorimeter, respectively. In all experiments, the concentration of HAN was kept around  $10^{-5}$  M. Double-distilled Mili-Q water was used to prepare the solutions for experiments. The time-resolved emission spectra were recorded using a TCSPC picosecond spectrophotometer. The details of the experimental setup for the picosecond TCSPC is described in our previous paper.<sup>80</sup> In brief, a picosecond diode laser at 375 nm (IBH, UK, Nanoled) was used as light source, and the signal was detected in magic angle ( $54.7^\circ$ ) polarization using a Hamamatsu MCP PMT (3809U). The typical instrument response function is 100 ps in our system. The decays were analyzed using IBH DAS-6 decay analysis software. The same software was also used for time-resolved anisotropy decay analysis. For steady-state anisotropy measurement, we used a Perkin-Elmer LS-55 luminescence spectrometer equipped with a filter polarizer and a thermostatted cell holder. All the experiments were performed at 25 °C.

The fluorescence quantum yield in different systems (micelles and niosomes) were determined using anthracene ( $\lambda_{\text{abs}} = 350$  nm) with absolute quantum yield of 0.27 in methanol at 25 °C as secondary standard. The following equation was used for calculation:

$$\frac{\Phi_S}{\Phi_R} = \frac{A_S}{A_R} \frac{(\text{Abs})_R}{(\text{Abs})_S} \frac{n_S^2}{n_R^2} \quad (1)$$

where  $\Phi$  represents the quantum yield, Abs represents the absorbance,  $A$  represents the area under the fluorescence curve, and  $n$  is the

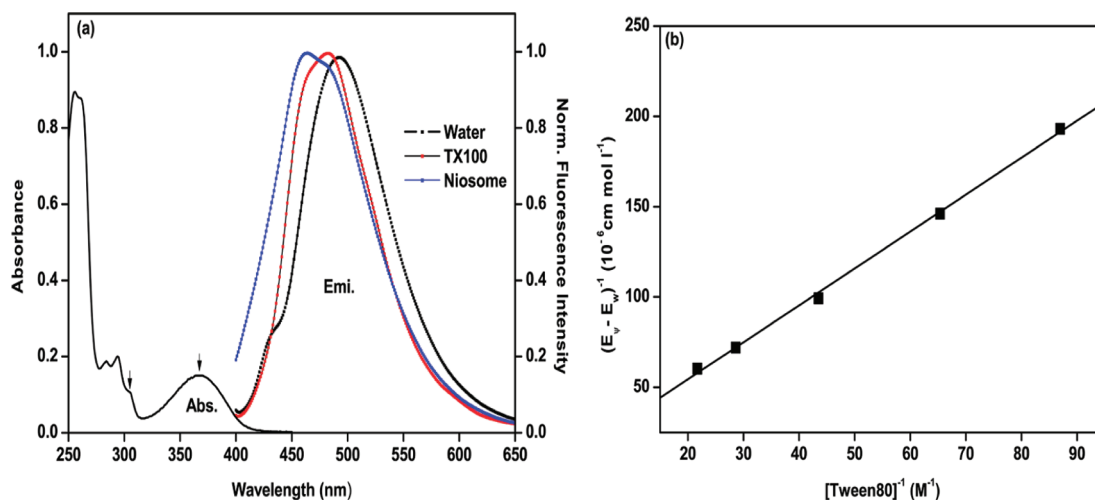


**Figure 1.** (a) UV–visible absorption (Abs) spectrum of HAN ( $10^{-5}$  M) in water (dashed line) and emission spectra of HAN in water (black squares) and in different supramolecular assemblies of TX100 (red squares) and niosomes (blue squares). (b) Plot of  $1/(E_v - E_w)$  vs  $[\text{Tween-80}]^{-1}$ .

refractive index of the medium. The subscripts S and R denote the corresponding parameters for the sample and reference, respectively.

**2.3. Preparation of Niosomes.** The stock niosome solution was prepared according to the literature procedure.<sup>26</sup> Briefly, Tween-80, PEG-6000, and water were vortex mixed at a certain molar fraction or at the mass ratio of 0.500/0.060/0.500, and then the mixture was sonicated for 25–30 min with the addition of 2 wt % aqueous solution of PEG-6000. Initially, the mixture forms a lamellar liquid crystal, and finally, after sonication on dilution with 2 wt % aqueous solution of PEG-6000, the niosomes were formed. These niosomes are multilamellar in nature, and the mean radius of the niosomes is 0.15–0.2  $\mu\text{m}$ . Niosomes in the Tween-80/PEG-6000/H<sub>2</sub>O systems are reported to be highly stable and have high dilution capability.<sup>27,28</sup>

**2.4. Viscosity Measurement.** Viscosity of the stock niosome solution was measured using a Brookfield DV-II+ Pro (viscometer) at 25 °C temperature. We have also determined the change of viscosity with the dilution of the niosome solution up to 4 times. All samples were kept for 24 h before the measurements to equilibrate. The measured values are given in Table 3.

### 3. RESULTS AND DISCUSSION

**3.1. Steady-State Absorption Studies.** In neutral water, the intramolecularly H-bonded closed enol conformer (E-II) of HAN absorbs at 368 nm. Theoretical study predicts that two water molecules can break the internal hydrogen bond of HAN.<sup>56</sup> So, in water, weakening of the intramolecular hydrogen bond may result in the formation of the open enol conformer, which gives rise to an additional absorption band shifted to shorter wavelength.<sup>76</sup> It may absorb at some wavelength between 300 and 368 nm as shown in Figure 1a. A similar observation has also been made for HNA in pure aqueous solvent. However, Guchhait et al. reported that the absorption band at 300 nm is responsible for the open conformer of HNA.<sup>20,21,70</sup> Gradual addition of surfactants, both ionic and nonionic, to the aqueous solution of HAN leads to the increase of absorbance at 368 nm along with slight red shift of the absorbance maxima (Figures S1 and S2, Supporting Information). The same observation is also found when the absorbance spectra of HAN are recorded in niosome solution varying the concentration of Tween-80 (Figure S3, Supporting

Information). Micelles and vesicles formed by surfactants provide a greater hydrophobic environment, which helps to solubilize and stabilize the enol form of HAN in the ground state and finally results the increment of absorbance. The relative red shift is due to the remarkable change in the micropolarity and rigidity of the heterogeneous micellar systems and niosomes compared with the homogeneous aqueous system. These altered properties of micelles and niosomes help to increase the strength of the intramolecular hydrogen bond of the ground state enol form by providing a greater hydrophobic environment and also by decreasing the number of water molecules involved in the intermolecular hydrogen bond. Increase in the intramolecular hydrogen bond strength means an increase in the electronic conjugation and hence the slight red shift. Therefore, restricted hydrophobic environments of micelles and vesicles stabilize the tautomers of HAN to a different extent leading to the perturbation of their ground- and excited-state energetics. This observation is consistent with the earlier observations in protein and other cavities.<sup>74,76,79</sup> HAN is reported to be a very useful probe as a polarity calibrator for different nanocavities because of its high sensitivity toward the polarity of the binding sites.<sup>67</sup> The absorption spectra of HAN in presence of increasing concentrations of surfactants are given in Supporting Information (Figures S2 and S3). The nature of the absorbance spectra (presence of an isosbestic type point) with the change of concentration of surfactants also indicates the presence of equilibrium between the microheterogeneous systems and free water near the CMC. This also indicates gradual incorporation of HAN in micelles and vesicles.

**3.2. Determination of Distribution Coefficient of HAN in Niosome.** The niosome is a better model of a membrane to bind a hydrophobic probe because it has hydrotrope-solubilizing action to hydrophilic as well as hydrophobic drugs.<sup>77,78</sup> In this case, there is a specific interaction between polymer (PEG-6000) and surfactant (Tween-80) that helps the formation of niosomes and makes the rigidity and stability of the niosome membrane where the probe molecule is basically confined. Here, using the UV–vis difference spectra of HAN in the niosome system, we have determined the distribution coefficient of HAN between the niosome heterogeneous phase and the water homogeneous phase.<sup>26</sup>

$$\frac{1}{E_v - E_w} = \frac{1}{K_D(E_m - E_w)} \frac{1}{c_S} + \frac{1}{E_m - E_w} \quad (2)$$

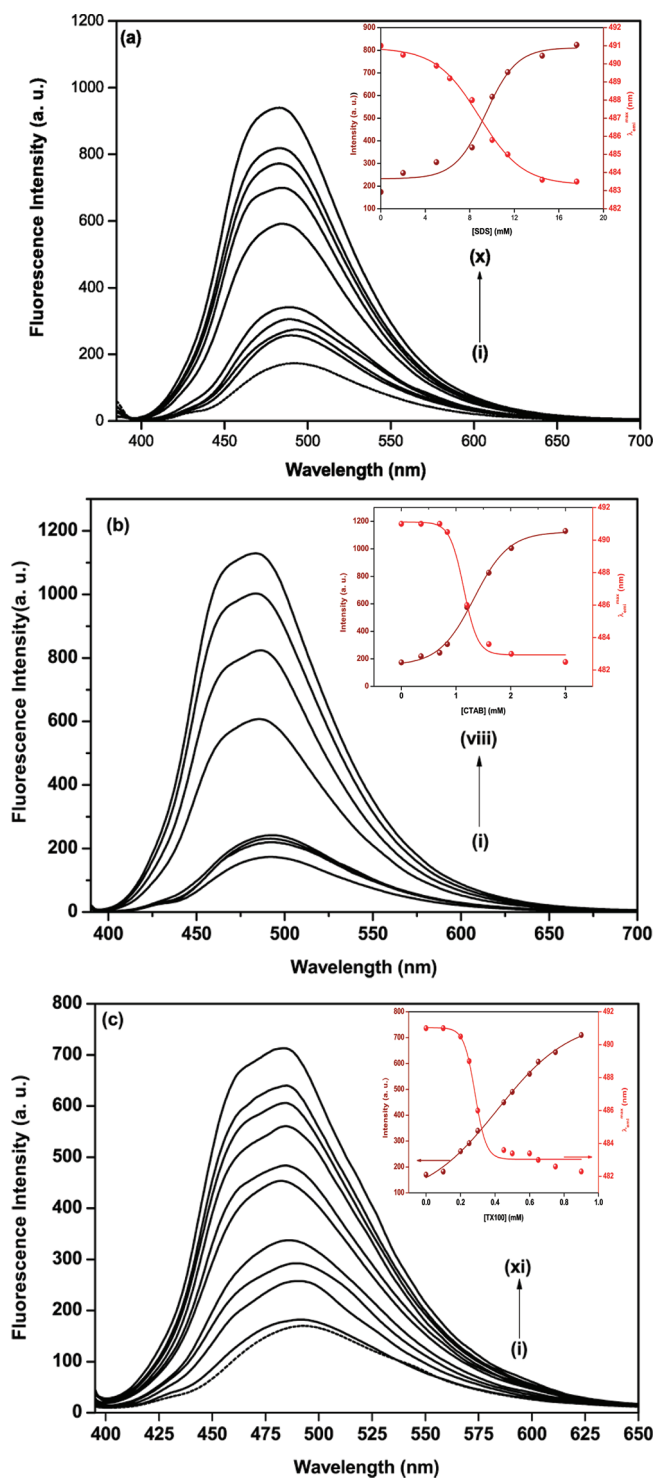


**Figure 2.** Emission spectra ( $\lambda_{\text{ex}} = 375 \text{ nm}$ ) of HAN in the presence of increasing concentration of (a) SDS [curves i–x correspond to concentration of SDS = 0, 2, 5, 6.2, 8.2, 10, 11.4, 14.5, 17.5, and 20 mM], (b) CTAB [curves i–viii correspond to concentration of CTAB = 0, 0.36, 0.7, 0.84, 1.2, 1.6, 2.01, and 3.0 mM] and (c) TX100 [curves i–xi correspond to 0, 0.1, 0.2, 0.25, 0.3, 0.45, 0.5, 0.6, 0.65, 0.75, and 0.9 mM]. The inset shows the variation of emission intensity at  $\lambda_{\text{em}} = 480 \text{ nm}$  and  $\lambda_{\text{max}}^{\text{emi}}$  of HAN with surfactant concentration.

where  $c_S$  is the surfactant concentration and  $E_\psi$  is the apparent mole absorption coefficient of HAN at a given wavelength obtained from

the absorption spectra on gradual addition of surfactant.  $E_w$  and  $E_m$  are the apparent mole absorption coefficients of HAN in the water continuous phase and in the niosome heterogeneous phase, respectively. Again  $E_w$  is obtained from the experiment in pure water. Now from the slope of the plot of  $1/(E_\psi - E_w)$  against  $1/c_S$  (Figure 1b),  $K_D$  was calculated. To do this experiment, we have varied the concentration of the surfactant Tween-80 through a dilution method of the stock niosome solution. The obtained value of  $K_D$  is  $4.89 \times 10^5$ , which indicates that the encapsulation efficiency of niosomes to the hydrophobic probe molecule (HAN) is high enough. Similarly high encapsulating efficiency of niosomes is observed when they bind with hydrophobic drug molecules.<sup>26</sup>

**3.3. Steady-State Emission Studies.** Fluorescence emission spectra of HAN in different micellar systems and in niosomes with varying concentrations of surfactants are recorded at the excitation wavelength of 375 nm. In neutral water, the emission spectrum of HAN is at 490 nm. But when it is encapsulated in the micellar systems, a significant enhancement in intensity along with  $\sim 10 \text{ nm}$  blue shift ( $425 \text{ cm}^{-1}$ ) is observed. The changes in the fluorescence intensity with the change in concentration of surfactants are depicted in Figure 2. The insets are given for understanding the variation of emission intensity and emission maxima as a function of surfactant concentration. From there, we have an idea about the critical micelle concentration (CMC) values of the individual surfactants because in each plot an inflection is observed at the CMC value of the surfactant. These experimental results match the reported CMC values. The blue shift indicates that the micropolarity sensed by the probe molecules in the micellar environment is less than the polarity of the bulk water because this type of blue shift is also observed in the solvents of lower polarity.<sup>71,72</sup> Catalan et al.<sup>67</sup> reported that solvatochromism of HAN is sensitive to the polarity of the cavity in which it is confined. The red shift of the PT emission increases as the polarity of the cavity increases. Therefore, the observed blue shift in different surfactant assemblies compared with water correlates well with the experimentally obtained equations by Catalan et al. A closer look at the fluorescence emission spectra of HAN in micelles, depicted in Figure 2, indicates that unlike in SDS micelles, the spectra are broader in case of CTAB and TX-100 micelles. This indicates that the binding of HAN inside SDS micelles is not as strong. The broadening of the spectra in CTAB and TX100 micelles comes from the greater heterogeneity of the sample in the excited state. The fluorescence quantum yield has also been found to be saturated on gradual increase with surfactant concentration. The increase in fluorescence quantum yield (given in Table 1) is due to the incorporation of the ground-state enol tautomer of HAN in micelles.<sup>45</sup> This behavior is very much expected because the ground-state enol form of HAN is reported to be very nonpolar having a dipole moment 2.99 D.<sup>69</sup>

For a better model to understand how the change of micro-polarity and rigidity of the heterogeneous systems affects the spectral behavior of HAN, we have used nonionic surfactants forming vesicles (niosomes). In niosomes, the emission spectrum of HAN is blue-shifted from 490 nm in water to 462 nm along with enhancement of fluorescence intensity. This observation is quite similar to the earlier observations of blue shift and enhancement of fluorescence quantum yield on addition of cyclodextrins (CDs),<sup>1–3,73–75</sup> modified CDs,<sup>76</sup> and human serum albumin (HSA).<sup>76</sup> In niosomes, a 28 nm blue shift ( $1237 \text{ cm}^{-1}$ ) with the appearance of an emission maximum at 462 nm clearly indicates a change in the photodynamics of HAN due to the effect of caging in the bilayer of the niosome. In TX100

**Table 1.** Binding Constants ( $K_1$ ), Free-Energy Changes for Interaction of HAN with Micelles and Niosomes, and Stern–Volmer Quenching Constant Values of HAN

samples	partition coefficient/ $K_1$ ( $10^5 \text{ M}^{-1}$ )	binding energy, $-\Delta G (\text{kJ mol}^{-1})$	$K_{sv}$ ( $10^3 \text{ M}^{-1}$ )
water			7.40
SDS	0.31	25.79	6.37
CTAB	3.30	31.69	1.28
TX100	2.90	31.37	2.85
niosomes	4.89 <sup>a</sup>	32.67	2.10

<sup>a</sup> Partition coefficient  $K_D$  of HAN in stock niosome solution obtained from the UV-vis difference spectra of HAN in niosome.

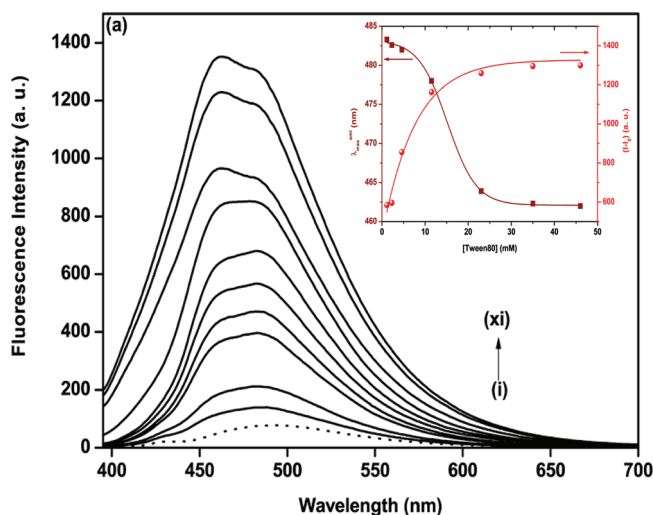


**Figure 3.** Emission spectra ( $\lambda_{\text{ex}} = 375 \text{ nm}$ ) of HAN in the presence of increasing concentration of Tween-80 [curves i–xi correspond to the concentration of Tween-80 in solution of 0, 0.23, 0.46, 0.69, 1.15, 2.3, 4.6, 11.5, 23, 35, and 46 mM]. The inset shows the variation of emission intensity at  $\lambda_{\text{em}} = 480 \text{ nm}$  and  $\lambda_{\text{max}}^{\text{emi}}$  of HAN with surfactant concentration.

micelles, we have found broad emission spectra (starting from 460 nm) with the emission maximum at 480 nm. Hence a large difference is observed in the niosome solution because the niosome membrane is comprised of the headgroups of nonionic surfactant Tween-80, which have a very long chain of oxyethylene units compared with TX100. Again, the surfactant PEG-6000 is the main component that enhances the rigidity and stability of the niosome.<sup>26–28</sup> Recently, Mahata et al.<sup>81</sup> have studied the photo-physics and rotational dynamics of  $\beta$ -carboline, showing the effect of variation of length of the head and tail part of nonionic surfactant. They have shown that the protection efficiency of the Tween series of surfactants is higher than that of the Triton X series of surfactants toward the probe molecules. Another interesting observation is that, as the niosome solution is diluted the emission spectra are found to be red-shifted with a decrease of the fluorescent intensity. The spectra are also found to be broadened (Figure 3). This may be attributed to the fact that the stability and number density of niosomes are affected by the dilution. Excessive dilution disrupts the niosome, and water molecules penetrate; hence the binding strength decreases. The normalized emission spectra of HAN in water and in heterogeneous systems of different binding capability are given in Figure 1a.

**3.4. Determination of HAN–Micelle Binding Constant.** Micelles and vesicles are common model systems to study the binding of many hydrophobic and hydrophilic small organic molecules. Depending on the nature of the probe molecule, the interaction with different supramolecular assemblies of surfactants will be different, and hence binding will be different. Here, in order to obtain a quantitative estimation of the binding interaction between HAN and micellar systems, the binding constants and the free energy change due to binding were determined using the method described by Almgren et al.<sup>82</sup> This method uses the following equation:

$$\frac{I_{\infty} - I_0}{I_t - I_0} = 1 + \frac{1}{K_1[M]} \quad (3)$$

In the above expression,  $I_0$ ,  $I_t$ , and  $I_{\infty}$  are the emission intensities of the probe molecule in the absence of surfactant (that is, in pure water), at different concentrations of surfactant, and at a condition of saturation, respectively.  $[M]$  denotes the concentration of micelle in solution. If the aggregation number of the micellar system at the surfactant concentration,  $[S]$ , and the CMC of the surfactant are known for that system, the micellar concentration can be determined from the following expression:

$$[M] = \frac{[S] - \text{CMC}}{N_{\text{agg}}} \quad (4)$$

The values of  $N_{\text{agg}}$  for SDS, CTAB, and TX-100 in water were taken from the reported values.<sup>83–85</sup> The linear plots of  $(I_{\infty} - I_0)/(I_t - I_0)$  vs  $[M]^{-1}$  for SDS, CTAB, and TX-100 micellar systems are shown in Figure 4. The binding constants were calculated from the slope, and the values are given in Table 1. The free energy change values due to the binding interaction are also given there. From the estimated values, it has been observed that the binding of HAN with the micelles of cationic (CTAB) and nonionic surfactant (TX-100) are greater than that with the micelles of anionic surfactant (SDS).

In order to achieve a better understanding and to support our experimental data, we have to take into account the theoretical data obtained from quantum mechanical calculation of HAN performed by A. V. Szeghalmi et al.<sup>61</sup> They have determined the partial electron charges ( $e$ ) within natural population analysis (NPA) at the CASSCF level. From there, it has been found that all the heteroatoms of HAN are endowed with partial negative charge. So SDS is expected to have poor binding capability with HAN compared with that of cationic and nonionic surfactants forming micelles, due to the repulsive force between the same types of charge in SDS micelles.

**3.5. Steady-State Fluorescence Anisotropy.** The steady-state fluorescence anisotropy was measured in niosome solutions with varying concentrations of Tween-80 to get an idea about the rigidity of the microenvironment surrounding the fluorophore. The concentration of Tween-80 was varied through gradual dilution of the stock niosome solution. Measurement of steady-state anisotropy with the varying concentration of Tween-80 will give information about the degree of rigidity of the microenvironment around the fluorophore. The steady-state anisotropy of HAN in water is 0.070, but in niosome solution, the anisotropy becomes 0.151, which reflects the increased rigidity of the microenvironment and the degree of binding efficiency. However, with the dilution of the niosome solution, that is with decreasing the concentration of Tween-80, the rigidity of the environment decreases and accordingly the anisotropy also decreases along

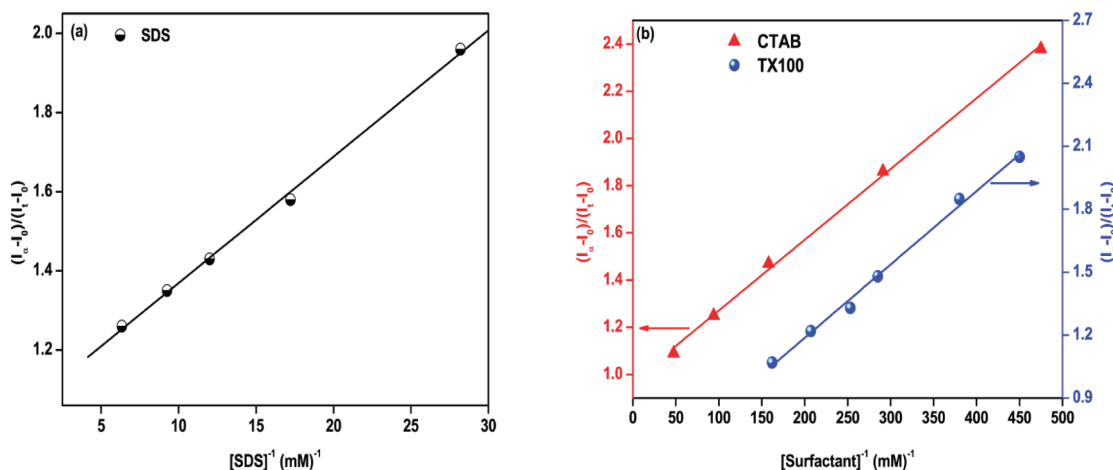


**Figure 4.** Plot of  $(I_{\infty} - I_0)/(I_t - I_0)$  vs (a)  $[SDS]^{-1}$  and (b)  $[CTAB]^{-1}$  and  $[TX100]^{-1}$ .

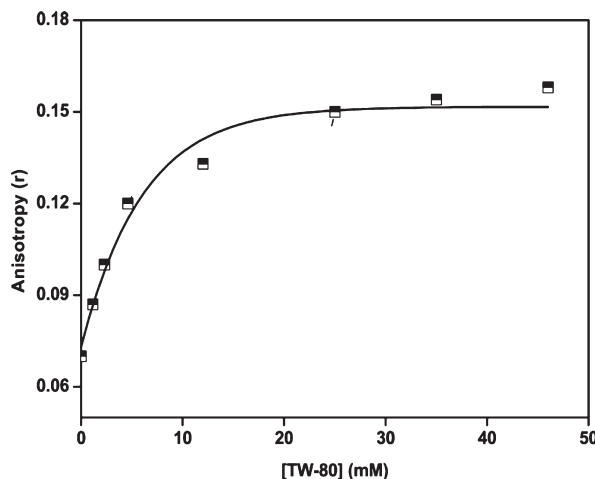


**Figure 5.** Change of steady-state fluorescence anisotropy with increasing concentration of Tween-80 in niosome solution of HAN.

with the observation of a sharp inflection point. This is because excessive dilution leads to the cleavage of niosome vesicles. This observation also provides an understanding about the compactness of the niosomes. Figure 5 depicts the change of fluorescence anisotropy of HAN as a function of Tween-80 concentration of the niosome solutions.

**3.6. Time-Resolved Emission Studies.** Time-resolved fluorescence decays of HAN in different solutions were recorded at excitation wavelength of 375 nm, and spectra were monitored at the emission wavelengths of 480 and 560 nm. The representative time-resolved fluorescence decay profile of HAN in micelles at 480 nm is depicted in Figure 6, and the corresponding lifetime values obtained from the multiexponential fitting of the decay are given in Table 2. Fluorescence lifetime measurements provide the information about the location of the probe when there is an option of partitioning the probe between homogeneous and heterogeneous phases. Depending on the partitioning of the fluorophore in confined systems like micelles and vesicles, a difference in the values of fluorescence lifetime is observed. For example, where the time-resolved emission decay of HAN in aqueous solution fits well to a biexponential function with time constants of  $\sim 90$  ps (99%) and  $\sim 4$  ns (1%), decays of HAN in

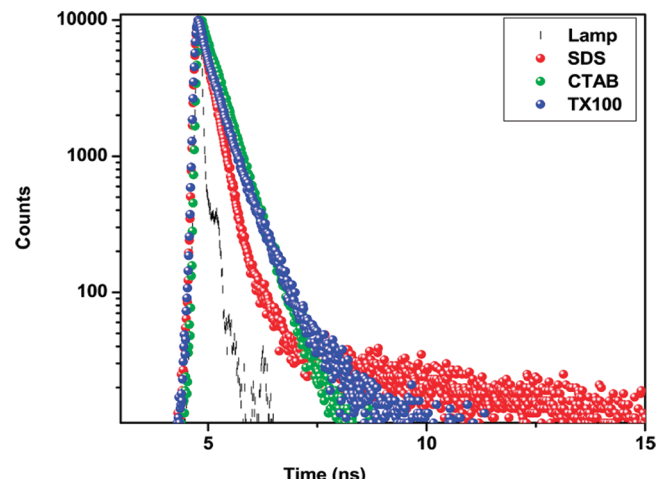


**Figure 6.** Time-resolved fluorescence decays of HAN in micellar systems of SDS (20 mM), CTAB (3 mM), and TX100 (1 mM) surfactants.

micelles (SDS/CTAB/TX100) fit well with a triexponential function. In aqueous solution, the major contributing fast component is attributed to the  $K^*$  form, and the minor contributing slow component is due to the normal enol tautomer emission. The major contribution from the PT tautomer ( $K^*$ ) can be explained on the basis of the observation of Moreno and Luch et al.<sup>59</sup> that on the  $S_1$  surface  $K^*$  seems to be more stable than  $E^*$ . The triexponential nature of the fluorescence decay of HAN in micellar systems is attributed to the binding of probe molecules; the shortest component is assigned to the free HAN in water, and the other two components having longer lifetime (picosecond and nanosecond) are assigned to the micelle-bound tautomers of HAN. The lifetime values of the probe confined in the micellar environment are significantly longer than those observed in pure homogeneous solvents.<sup>71</sup> The lifetime values in the CTAB micellar system are 96 ps, 360 ps, and 1.50 ns and those values in TX100 micelles 108 ps, 417 ps, and 1.63 ns. The increased lifetime value of the shortest component from 90 ps in pure water to 96 ps in CTAB and 108 ps in TX100 is due to the increase in the viscosity of the medium upon addition of surfactants. Because the microviscosity around the fluorophore

**Table 2.** Fluorescence Lifetime and Quantum Yield ( $\Phi_f$ ) and Radiative and Nonradiative Rate Constants of HAN in Water and Different Micelles<sup>a</sup>

environments	$\tau_1$ , ns ( $a_1$ )	$\tau_2$ , ns ( $a_2$ )	$\tau_3$ , ns ( $a_3$ )	$\langle \tau_f \rangle$ , ns	$\Phi_f$	$k_r (10^8 \text{ s}^{-1})$	$k_{nr} (10^9 \text{ s}^{-1})$
water	0.09 (0.99)	4.0 (0.01)		0.129	0.007	0.54	7.70
SDS	0.097 (0.34)	0.257 (0.65)	5.58 (0.01)	0.256	0.027	1.05	3.80
CTAB	0.096 (0.39)	0.360 (0.59)	1.50 (0.02)	0.280	0.026	0.93	3.47
TX100	0.108 (0.42)	0.417 (0.56)	1.63 (0.02)	0.311	0.031	0.99	3.10

<sup>a</sup> Experimental error  $\pm 5\%$ .

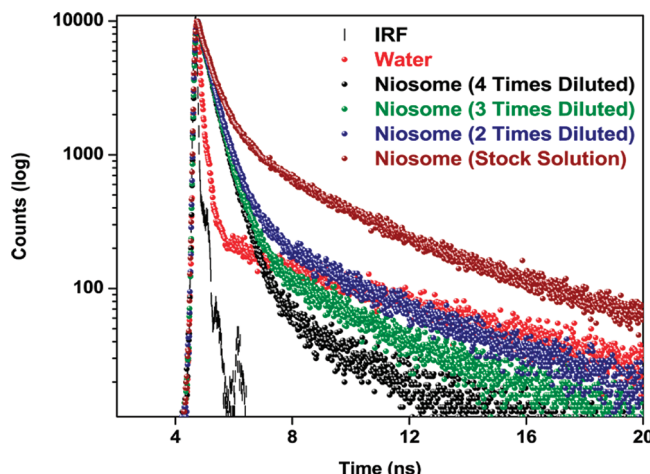


**Figure 7.** Time-resolved fluorescence decays of HAN in niosome solutions having different concentrations of Tween-80 obtained through the dilution of stock niosome solution with pure water up to 4 times.

in TX100 micellar solution is greater than that in CTAB micellar solution, the difference in the lifetime values of free HAN is observed. The longer picosecond component, that is, the component having lifetime of 360 ps in CTAB micelles and 417 ps in TX100 micelles, seems attributable to the encapsulated PT tautomer ( $K^*$ ) in micelles. In analogy with the previously reported results, we have assigned the particular lifetime components of HAN in micellar systems. The reason is that the contribution (pre-exponential factor) of shortest component decreases from 99% in pure water to 42% in TX100 micelles and 39% in CTAB micelles, which is attributed to the incorporation of HAN in micellar assemblies. Again the contribution of the 417 ps component in TX100 micelles, which is assigned to the encapsulated  $K^*$  decreases from 42% to 32% with increasing the contribution of free HAN (fast component) when emission wavelength changes from 480 to 560 nm, respectively. This observation also seems reasonable because free HAN in water emits at the red end and encapsulated HAN exhibits blue-shifted emission. These observations comply with earlier observations in cyclodextrins and the HSA microenvironment. However, in such heterogeneous micellar systems, it is very difficult to assign individual decay time constants. Therefore, instead of giving too much importance to the individual decay time constants in these heterogeneous systems, we have determined the mean fluorescence lifetime to explain the dynamical behavior of HAN. The calculated values of the average fluorescence lifetimes are given in Table 2. The lifetime value of this micelle-bound component is largely influenced by the protection efficiency of the heterogeneous systems; the stronger the protection, the longer will be the lifetime values. Interestingly, we observed

**Table 3.** Fluorescence Lifetime and Quantum Yield of HAN in Niosome Solutions with Varying Concentration of TW-80 and Viscosity of the Solution<sup>a</sup>

HAN in niosomes of stock/water (v/v)	$\tau_1$ , ns ( $a_1$ )	$\tau_2$ , ns ( $a_2$ )	$\tau_3$ , ns ( $a_3$ )	viscosity ( $\eta$ , cP)
1:3	0.150 (0.32)	0.430 (0.66)	2.37 (0.02)	0.95
1:2	0.150 (0.26)	0.430 (0.71)	2.37 (0.03)	1.00
1:1	0.196 (0.24)	0.444 (0.71)	2.57 (0.05)	1.02
1:0	0.196 (0.24)	0.444 (0.64)	2.57 (0.12)	1.36

<sup>a</sup> Experimental error  $\pm 5\%$ .

triexponential decay in SDS micelles with time constants 97 ps, 257 ps, and 5.58 ns. The presence of a long-lived nanosecond component indicates that in SDS micelles probe molecules are highly exposed to water. We have already obtained an indication of this type of behavior from the steady-state emission spectra of HAN in SDS systems. We have discussed that the penetrating power of HAN in SDS micelles is not so strong, that means the heterogeneity of the sample in SDS micellar solution is minimal. The majority of the probe is exposed to water. This observation complies with the earlier observation in  $\gamma$  CD, where greater size of the nanocavity results in less protection of the probe.

We have also recorded the emission decays of HAN in stock niosome solution and also in niosome solutions of various concentrations of Tween-80 obtained through the dilution of stock niosome solution up to 4 times in different ratios of stock and water (v/v) (Figure 7). The emission decays were fitted to a triexponential function, and the lifetime values of the three components are given in Table 3. We obtained the time constants for HAN in stock niosome solution as 196 ps (24%), 444 ps (64%), and 2.57 ns (12%). These components are longer than those previously obtained in micellar solutions. This reflects the stronger binding efficiency of niosomes toward HAN. However, they are very similar to the components reported for the binding of HAN with HSA.<sup>76</sup> The lifetime values of the excited-state tautomers are guided by the caging in the media. Therefore, in niosomes the contribution to the signal of the slow component, that is, the nanosecond component, increases from 1% in pure water to 5% in the 2 times diluted niosome solution, and finally 12% in the stock niosome solution. This observation is due to the enhanced caging of HAN in niosomes. Another interesting point to note is that the value of the pre-exponential factors of all these components depend on the relative concentration of the surfactant (Tween-80) and on the monitored emission wavelength. For example, in the 2 times diluted niosome solution, the emission decay of HAN at 480 nm gives time constants 196 ps (24%), 444 ps (71%), and 2.5 ns (5%), whereas the emission

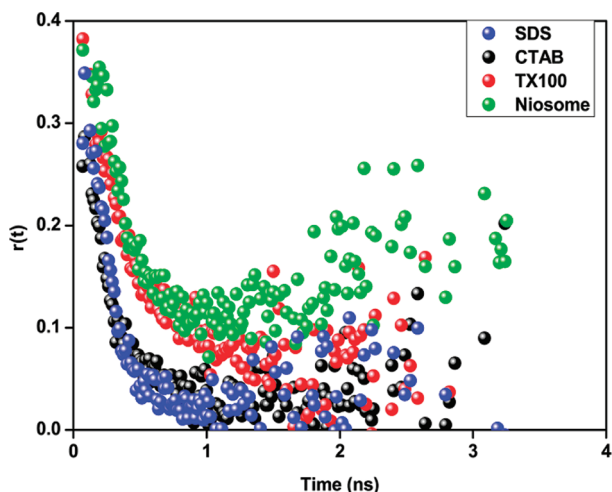


**Figure 8.** Time-resolved fluorescence anisotropy decays of HAN in micellar media of SDS, CTAB, and TX100 surfactants and in the solution of niosomes.

decay at 560 nm gives the time constants 196 ps (35%), 446 ps (59%), and 2.5 ns (6%). Therefore, as the emission wavelength changes from 480 to 560 nm, the contribution of free HAN increases. Again, in general when the concentration of surfactant increases (i.e., changing the medium from 4 times diluted niosome solution to stock niosome solution) the contribution of free HAN decreases and that of encapsulated tautomers increases. The reason is that as the niosome solution is being diluted more water molecules penetrate and hence the binding efficiency decreases. It is reported<sup>26–28</sup> that 4 times dilution of the stock niosome solution does not disrupt the niosome, and it can be stable for more than 50 h.

To further interpret the time-resolved emission decay results and to get a better idea about the modulation in the excited state behavior of HAN upon encapsulation we have calculated the radiative and nonradiative decay rate constants using the following equations:

$$k_r = \frac{\Phi_f}{\langle \tau \rangle_f} \quad (5)$$

$$k_{nr} = \frac{1}{\langle \tau \rangle_f} - k_r \quad (6)$$

where  $k_r$  and  $k_{nr}$ , respectively, represent the radiative and nonradiative rate constants. The calculated values are given in Table 2. The radiative and nonradiative processes are accordingly modified with the change in the fluorescence lifetime and hence with the caging of the environment. From Table 2, it is evident that in pure aqueous solution the nonradiative rate constant of HAN is very high  $\sim 7.7 \times 10^9 \text{ s}^{-1}$ . Similar high nonradiative rate constants are also observed in different hydrogen bonding solvents where the  $k_{nr}$  value increases with increasing the solvent polarity.<sup>71</sup> The  $k_{nr}$  value is reduced with increasing effect of confinement. The nonradiative rate of HAN in micelles is  $\sim 3 \times 10^9 \text{ s}^{-1}$ , whereas in niosomes the value is  $1.48 \times 10^9 \text{ s}^{-1}$ . Now, the enhanced fluorescence intensity along with longer emission lifetime in niosomes, as well as micelles, compared with pure aqueous solution is consistent with the

**Table 4. Dynamic Parameters of Fluorescence Anisotropy of HAN in Micelles and in Niosomes<sup>a</sup>**

environments	$a_{1r}$	$\tau_{1r}$ (ns)	$a_{2r}$	$\tau_{2r}$ (ns)	$\langle \tau_r \rangle$ (ns)	$\chi^2$
SDS	0.90	0.180	0.10	1.10	0.272	1.2
CTAB	0.73	0.150	0.27	1.30	0.460	1.19
TX100	0.71	0.235	0.29	1.74	0.671	1.11
niosome	0.63	0.267	0.37	1.64	0.775	1.26

<sup>a</sup> Experimental error  $\pm 5\%$ .

decrease in the nonradiative decay channels in these restricted environments.

**3.7. Time-Resolved Anisotropy Study.** For better understanding about the microenvironment surrounding the probe and also the binding ability of the systems, time-resolved fluorescence anisotropy of HAN was recorded in micelles and niosomes. Time-resolved fluorescence anisotropy,  $r(t)$ , was calculated using the following equation:

$$r(t) = \frac{I_{||}(t) - GI_{\perp}(t)}{I_{||}(t) + 2GI_{\perp}(t)} \quad (7)$$

where  $G$  is the correction factor for detector sensitivity to the polarization direction of the emission.  $I_{||}(t)$  and  $I_{\perp}(t)$  are the fluorescence decays polarized parallel and perpendicular to the polarization of the excitation light, respectively. Figure 8 shows representative anisotropy decays at 480 nm in micelles (SDS/CTAB/TX100) and in niosomes. In pure aqueous medium, the anisotropy decay is reported to be single exponential, and it is  $\sim 75$  ps.<sup>70</sup> However, in micellar solution as well as in niosomes, the time-resolved anisotropy decays are found to be biexponential. Thus time-resolved anisotropy measurements provide important information about the location of the probe molecules because the shortest component is attributed to the free HAN in solution and the longer time constant is attributed to the micelle- or vesicle-bound HAN. Therefore, in micelles as well as in niosomes, the probe molecules are motionally restricted. All the decay parameters in aqueous as well as aqueous micellar and niosome solutions are given in Table 4. The results indicate that HAN exhibits slower fluorescence anisotropy in niosome solution than it does in micelles. Again the anisotropy decays in these different organized assemblies are comparatively much slower than those in pure aqueous solution. This is attributed to the stronger binding of the probe molecule in niosomes than in micelles. Membrane-bound probes often display unusual behavior in which the anisotropy decays do not recover to zero.<sup>88</sup> This is because some probes do not rotate freely in the membrane and the extent of rotation is often limited by the compactness and the rigidity of the environment in which the probe is confined. The non-zero anisotropies at long times can be interpreted in terms of the order parameters ( $S$ ) of the membrane. The higher the order parameter, the higher is the rigidity of the microenvironment around the probe molecule. Therefore, in order to get further information about the rotational restriction on probe molecule (HAN) confined in micelles and niosomes, we have calculated the generalized order parameter ( $S$ ) using the following equation:

$$S^2 = a_{2r} \quad (8)$$

where  $a_{2r}$  is the relative amplitude of the slow component. The value of  $S$  ranges from 0 (for unrestricted motion) to 1 (for completely restricted motion). The order parameter in the

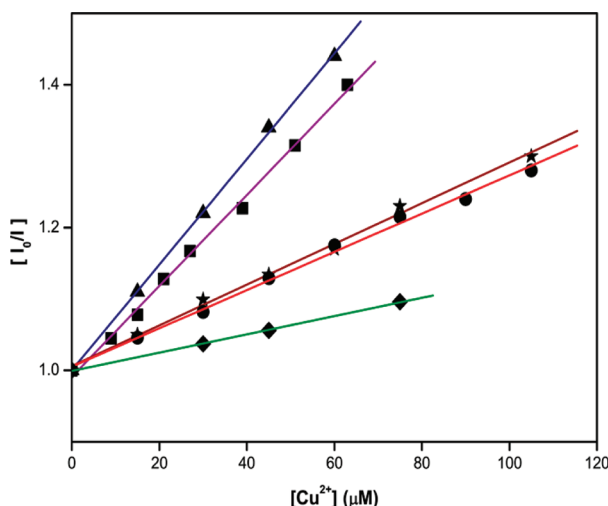


**Figure 9.** Stern–Volmer plots for the steady-state fluorescence quenching of HAN by Cu<sup>2+</sup> ions in water ( $\blacktriangle$ ) and in the presence of different microenvironments of SDS ( $\blacksquare$ ), CTAB ( $\blacklozenge$ ), and TX100 ( $\star$ ) micelles and in niosome solution ( $\bullet$ ).

niosome system is found to be 0.61 and that in TX100 micellar media 0.54, whereas in SDS and CTAB micelles, the order parameters are 0.32 and 0.51, respectively. These high values of order parameters in niosomes and TX100 compared with SDS and CTAB may be the reason why anisotropy decays of HAN in niosomes and TX100 do not recover to zero. Moreover, the initial anisotropy,  $r(0)$ , values of HAN in CTAB and SDS micellar solutions are lower than the ideal 0.4. This is may be due to the involvement of some ultrafast process for the free HAN molecules.

**3.8. Metal Ion Induced Fluorescence Quenching Study.** In recent literature,<sup>86,87</sup> the metal ion Cu<sup>2+</sup> has been used extensively for studying the fluorescence quenching of a probe molecule bound in different supramolecular assemblies. The main aim to this experiment is to get an idea about the location of the probe molecule and the protection efficiency of the systems.<sup>88</sup> We have investigated the steady-state fluorescence quenching of micelle- and vesicle-bound HAN using Cu<sup>2+</sup>, a heavy metal ion quencher, to see how the accessibility of host (HAN) by the quencher differs in different microenvironments. The nature of surfactant also plays an important role for the accessibility of Cu<sup>2+</sup> in micellar environments. The main idea comes from the fact that the ionic quencher Cu<sup>2+</sup> is not supposed to be present in the hydrophobic core of micelles and niosomes but it is supposed to be present in the water continuous phase as well as in the polar stern layer of micelles and the bilayer of niosomes. Moreover, for the micelles of ionic surfactant, the charge of the headgroup also plays an important role in bringing the metal ion quencher to the stern layer of micelles. The quenching rate constants for the different systems were determined using the Stern–Volmer relation where the terms have their usual meanings:

$$\frac{F_0}{F} = 1 + K_{sv}[Q] \quad (9)$$

The Stern–Volmer plots for the quenching of HAN in different micellar environments and in niosome solution have been given in Figure 9. The slope of each plot provides the Stern–Volmer quenching constant ( $K_{sv}$ ), and the values are given in Table 1. From the experimental results, we have found that the quenching

is very much faster for the SDS micellar environment compared with the other supramolecular assemblies. This is due to the stronger interaction between Cu<sup>2+</sup> ion and the anionic headgroup of SDS. This is supported by the finding of Konuk et al. and others.<sup>89,90</sup> To avoid any structural change induced in micellar aggregates of SDS by strong binding of Cu<sup>2+</sup> ions, the concentration of the quencher has been taken in micromolar range. The quenching is least for the system of CTAB micelles where the cationic headgroup prevents the approach of Cu<sup>2+</sup> in the stern layer. The observation of quenching in the micellar solution and in niosomes suggests that the probe is located in the stern layer of ionic micelles, palisade layer of nonionic micelles, and bilayer of niosomes. The accessibility of the quencher toward the probe molecules in these supramolecular assemblies depends upon the surface charge of the micelle. For the systems of nonionic surfactant, the quenching is controlled by the binding efficiency and compactness of the systems.<sup>81</sup>

#### 4. CONCLUSION

In this study, we have reported on modulation of photophysics and photodynamics of HAN in different biologically relevant supramolecular assemblies of micelles and vesicles formed by surfactant aggregates. The hydrophobic and confined environments provided by micelles and niosomes help to bind the tautomers of HAN and result in an increase in the fluorescence quantum yield with longer lifetime of the caged tautomers. This work demonstrates a comparative study on the binding efficiency of the different assemblies depending on the nature of microenvironments toward HAN. The more rigid and confined environment provided by niosomes results in longer lifetimes of caged tautomers (444 ps and 2.57 ns) than those found in micelles. Among the micelles, cationic and nonionic micelles have higher binding efficiency than SDS micelles, and this finding is supported by both steady-state and time-resolved experiments and also by the previously reported theoretical results. Again the steady-state quenching experiment by heavy metal ion quencher Cu<sup>2+</sup> also reveals that the protection efficiency of niosomes for HAN is higher than the protection efficiency provided by TX100 micelles. The higher encapsulation efficiency of niosomes for HAN may further promote its potential applicability as a drug carrier.

#### ■ ASSOCIATED CONTENT

**S Supporting Information.** Information on the change in the UV–visible absorption spectra of HAN in micelles and niosomes upon gradual addition of surfactant. This material is available free of charge via the Internet at <http://pubs.acs.org>.

#### ■ AUTHOR INFORMATION

##### Corresponding Author

\*E-mail: nilmoni@chem.iitkgp.ernet.in. Fax: 91-3222-255303.

#### ■ ACKNOWLEDGMENT

N.S. is thankful to Council of Scientific and Industrial Research (CSIR) and Board of Research in Nuclear Sciences (BRNS), Government of India, for generous research grants. S.M., V.G.R., C.G., and R.P. are thankful to CSIR for a research fellowship. S.S. is thankful to BRNS for a SRF.

## ■ REFERENCES

- (1) Douhal, A. *Chem. Rev.* **2004**, *104*, 1955–1976.
- (2) Douhal, A. *Acc. Chem. Res.* **2004**, *37*, 349–355.
- (3) Douhal, A.; Fiebig, T.; Chachisvilis, M.; Zewail, A. H. *J. Phys. Chem. A* **1998**, *102*, 1657–1660.
- (4) Bhattacharyya, K. *Acc. Chem. Res.* **2003**, *36*, 95–101.
- (5) Mondal, S. K.; Sahu, K.; Sen, P.; Roy, D.; Ghosh, S.; Bhattacharyya, K. *Chem. Phys. Lett.* **2005**, *412*, 228–234.
- (6) Mondal, S. K.; Sahu, K.; Ghosh, S.; Sen, P.; Bhattacharyya, K. *J. Phys. A* **2006**, *110*, 13646–13652.
- (7) Abou-Zied, O. K. *J. Phys. Chem. B* **2007**, *111*, 9879–9885.
- (8) Abou-Zied, O. K. *J. Phys. Chem. B* **2010**, *114*, 1069–1076.
- (9) Mojumdar, S.; Mondal, S.; Das, T.; Dey, A. K.; Bhattacharyya, K. *J. Chem. Phys.* **2010**, *132*, No. 194505.
- (10) Politis, M. J.; Brandt, O.; Fendler, J. H. *J. Phys. Chem.* **1985**, *89*, 2345–2354.
- (11) Gutman, M. *Adv. Chem.* **1994**, *235*, 27–40.
- (12) Adhikary, R.; Carlson, P. J.; Kee, T. W.; Petrich, J. W. *J. Phys. Chem. B* **2010**, *114*, 2997–3004.
- (13) Sarkar, N.; Das, K.; Das, S.; Datta, A.; Nath, D.; Bhattacharyya, K. *J. Phys. Chem.* **1995**, *99*, 17711–17714.
- (14) Chattopadhyay, N.; Dutta, R.; Chowdhury, M. *J. Photochem. Photobiol. A* **1989**, *47*, 249–257.
- (15) Cohen, B.; Huppert, D.; Solntsev, K. M.; Tsafadia, Y.; Nachliel, E.; Gutman, M. *J. Am. Chem. Soc.* **2002**, *124*, 7539–7547.
- (16) Choudhury, S. D.; Pal, H. *J. Phys. Chem. B* **2009**, *113*, 6736–6744.
- (17) Sarkar, N.; Datta, A.; Das, S.; Das, K.; Bhattacharyya, K. *J. Photochem. Photobiol. A* **1997**, *109*, 259–265.
- (18) Choudhury, S. D.; Nath, S.; Pal, H. *J. Phys. Chem. B* **2008**, *112*, 7748–7753.
- (19) Mondal, T.; Das, A. K.; Sasmal, D. K.; Bhattacharyya, K. *J. Phys. Chem. B* **2010**, *114*, 13136–13142.
- (20) Il'ichev, Y. V.; Solntsev, K. M.; Kuzmin, M. G.; Lemmetyinen, H. *J. Chem. Soc., Faraday Trans.* **1994**, *90*, 2717–2724.
- (21) Paul, B. K.; Guchhait, N. *J. Phys. Chem. B* **2010**, *14*, 12528–12540.
- (22) Ramamurthy, V., Ed. *Photochemistry in Organized and Constrained Media*; VCH: New York, 1991.
- (23) D'Souza, V. T.; Lipkowitz, K. B. *Chem. Rev.* **1998**, *98*, 1741.
- (24) John, V. T.; Blake, S.; McPherson, G. L.; Bose, A. *Curr. Opin. Colloid Interface Sci.* **2002**, *7*, 288–295.
- (25) Langevin, D. *Stud. Surf. Sci. Catal.* **1998**, *117*, 129–134.
- (26) Liu, T.; Guo, R. *Langmuir* **2005**, *21*, 11034–11039.
- (27) Liu, T.; Guo, R. *Colloid Polym. Sci.* **2007**, *285*, 711–713.
- (28) Liu, T.; Guo, R.; Hua, W.; Qiu, J. *Colloids Surf., A* **2007**, *293*, 255–261.
- (29) Bagchi, B. *Chem. Rev.* **2005**, *105*, 3197–3218.
- (30) Pal, S.; Zewail, A. H. *Chem. Rev.* **2004**, *104*, 2099–2123.
- (31) Mondal, J. A.; Nihonyanagi, S.; Yamaguchi, S.; Tahara, T. *J. Am. Chem. Soc.* **2010**, *132*, 10656–10657.
- (32) Nagayasu, A.; Uchiyama, K.; Kiwada, H. *Adv. Drug Delivery Rev.* **1999**, *40*, 75–87.
- (33) Schreier, H.; Bouwstra, J. *J. Controlled Release* **1994**, *30*, 1–15.
- (34) Svenson, S. *Carrier-Based Drug Delivery*; ACS Symposium Series, Vol. 879; American Chemical Society: Washington, DC, 2004.
- (35) Patel, R. P. *Niosomes: An Unique Drug Delivery System*. Pharmainfo.net, 2007.
- (36) Weller, A. H. *Prog. React. Kinet.* **1961**, *1*, 187–214.
- (37) Beens, H.; Grellmann, K. H.; Gurr, M.; Weller, A. H. *Discuss. Faraday Soc.* **1965**, *39*, 183–193.
- (38) Takeuchi, S.; Tahara, T. *J. Phys. Chem. A* **1998**, *102*, 7740–7753.
- (39) Takeuchi, S.; Tahara, T. *J. Phys. Chem. A* **2005**, *109*, 10199–10207.
- (40) Catalán, J.; Diaz, C.; Perez, P.; De Paz, L. G. *J. Phys. Chem. A* **2006**, *110*, 9116–9122.
- (41) Bhattacharya, B.; Samanta, A. *J. Phys. Chem. B* **2008**, *112*, 10101–10106.
- (42) Adhikary, R.; Mukherjee, P.; Kee, T. W.; Petrich, J. W. *J. Phys. Chem. B* **2009**, *113*, 5255–5261.
- (43) Catalán, J. *J. Phys. Chem. A* **2010**, *114*, 811–816.
- (44) Chen, Y.; Gai, F.; Petrich, J. W. *J. Am. Chem. Soc.* **1993**, *115*, 10158–10166.
- (45) De, D.; Datta, A. *J. Phys. Chem. B* **2010**, *115*, 1032–1037.
- (46) Douhal, A.; Kim, S. K.; Zewail, A. H. *Nature* **1995**, *378*, 260–263.
- (47) Gil, M.; Ziolkiewicz, M.; Organero, J. A.; Douhal, A. *J. Phys. Chem. C* **2010**, *114*, 9554–9562.
- (48) Seo, J.; Kim, S.; Park, S. Y. *J. Am. Chem. Soc.* **2004**, *126*, 11154–11155.
- (49) Solntsev, K. M.; Clower, C. E.; Tolbert, L. M.; Huppert, D. *J. Am. Chem. Soc.* **2005**, *127*, 8534–8544.
- (50) Banerjee, S.; Pabbathi, A.; Sekhar, M. C.; Samanta, A. *J. Phys. Chem. B* **2011**, *115*, 9217–9225.
- (51) Luiz, M.; Biasutti, A.; Soltermann, A. T.; Garcia, N. A. *Polym. Degrad. Stab.* **1999**, *63*, 447–453.
- (52) Sun, W.; Li, S.; Hu, R.; Qian, Y.; Wang, S.; Yang, G. *J. Phys. Chem. A* **2009**, *113*, 5888–5895.
- (53) Wu, J.; Liu, W.; Ge, J.; Zhang, H.; Wang, P. *Chem. Soc. Rev.* **2011**, *40*, 3483–3495.
- (54) Sobolewski, A. L.; Domcke, W. *Phys. Chem. Chem. Phys.* **2006**, *8*, 3410–3417.
- (55) Service, R. F. *Science* **2005**, *310*, 1762–1763.
- (56) Organero, J. A.; Garcia-Ochoa, I.; Moreno, M.; Lluch, J. M.; Santos, L.; Douhal, A. *Chem. Phys. Lett.* **2000**, *328*, 83–89.
- (57) Douhal, A.; Lahmani, F.; Zehnacker-Rentien, A. *Chem. Phys.* **1993**, *178*, 493–504.
- (58) Organero, J. A.; Moreno, M.; Santos, L.; Lluch, J. M.; Douhal, A. *J. Phys. Chem. A* **2000**, *104*, 8424–8431.
- (59) Ortiz-Sánchez, J. M.; Gelabert, R.; Moreno, M.; Lluch, M. *J. Chem. Phys.* **2007**, *127*, No. 084318.
- (60) Douhal, A.; Lahmani, F.; Zewail, A. *Chem. Phys.* **1996**, *207*, 477–498.
- (61) Szeghalmi, A. V.; Engel, V.; Zgierski, Z. M.; Popp, J.; Schmitt, M. *J. Raman Spectrosc.* **2006**, *37*, 148–160.
- (62) Lu, C.; Hsieh, R. M. R.; Lee, I. R.; Cheng, P. Y. *Chem. Phys. Lett.* **1999**, *310*, 103–110.
- (63) Lochbrunner, S.; Schultz, T.; Schmitt, M.; Shaffer, J. P.; Zgierski, M. Z.; Stolow, A. *J. Chem. Phys.* **2001**, *114*, 2519–2522.
- (64) Organero, J. A.; Vargas Diaz, A.; Moreno, M.; Santos, L.; Douhal, A. *J. Phys. Chem. A* **2001**, *105*, 7317–7320.
- (65) Tobita, S.; Yamamoto, M.; Kurahayashi, N.; Tsukagoshi, R.; Nakamura, Y.; Shizuka, H. *J. Phys. Chem. A* **1998**, *102*, 5206–5214.
- (66) Catalán, J.; Del Valle, J. C. *J. Am. Chem. Soc.* **1993**, *115*, 4321–4325.
- (67) Catalán, J.; Del Valle, J. C.; Diaz, C.; Palomar, J.; De Paz, J. L. G.; Kasha, M. *Int. J. Quantum Chem.* **1999**, *72*, 421–438.
- (68) Catalán, J.; De Paz, J. L. G. *J. Phys. Chem. A* **2001**, *105*, 7315–7316.
- (69) Catalán, J.; De Paz, J. L. G. *J. Phys. Chem. A* **2008**, *112*, 904–914.
- (70) Singh, R. B.; Mahanta, S.; Kar, S.; Guchhait, N. *Chem. Phys.* **2007**, *331*, 373–384.
- (71) Organero, J. A.; Douhal, A. *Chem. Phys. Lett.* **2003**, *381*, 759–765.
- (72) Lochbrunner, S.; Szeghalmi, A.; Stock, K.; Schmitt, M. *J. Chem. Phys.* **2005**, *122*, No. 244315.
- (73) Organero, J. A.; Santos, L.; Douhal, A. In *Femtochemistry and Femtobiology: Ultrafast Dynamics in Molecular Science*; Douhal, A., Santamaría, J., Eds.; World Scientific: Singapore, 2002; p 225.
- (74) Organero, J. A.; Tormo, L.; Douhal, A. *Chem. Phys. Lett.* **2002**, *363*, 409–414.
- (75) Organero, J. A.; Douhal, A. *Chem. Phys. Lett.* **2003**, *373*, 426–431.
- (76) Organero, J. A.; Martin, C.; Cohen, B.; Douhal, A. *Langmuir* **2008**, *24*, 10352–10357.
- (77) Girigovindam, A.; Das, S.; De, S. *Spectrochim. Acta, Part A* **2006**, *64*, 859–866.

- (78) Hao, Y.; Zhao, F.; Li, N.; Yang, Y.; Li, K. *Int. J. Pharm.* **2002**, 244, 73–80.
- (79) Banerjee, D.; Pal, S. K. *Chem. Phys. Lett.* **2008**, 451, 237–242.
- (80) Seth, D.; Chakrabarty, D.; Chakraborty, A.; Sarkar, N. *Chem. Phys. Lett.* **2005**, 401, 546–552.
- (81) Mahata, A.; Sarkar, D.; Bose, D.; Ghosh, D.; Girigoswami, A.; Das, P.; Chattopadhyay, N. *J. Phys. Chem. B* **2009**, 113, 7517–7526.
- (82) Almgren, M.; Grieser, F.; Thomas, J. K. *J. Am. Chem. Soc.* **1979**, 101, 279–291.
- (83) Weidemaier, K.; Tavernier, H. L.; Fayer, M. D. *J. Phys. Chem. B* **1997**, 101, 9352–9361.
- (84) Snyder, S. W.; Buell, S. L.; Demas, J. N.; DeGraff, B. A. *J. Phys. Chem.* **1989**, 93, 5265–5271.
- (85) Law, K. Y. *Photochem. Photobiol.* **1981**, 33, 799–806.
- (86) Mallick, A.; Mandal, M. C.; Haldar, B.; Chakrabarty, A.; Das, P.; Chattopadhyay, N. *J. Am. Chem. Soc.* **2006**, 128, 3126–3127.
- (87) Mallick, A.; Mandal, M. C.; Haldar, B.; Chakrabarty, A.; Das, P.; Chattopadhyay, N. *J. Am. Chem. Soc.* **2006**, 128, 10629–10629.
- (88) Lakowicz, J. R. *Principles of Fluorescence Spectroscopy*, 3rd ed.; Plenum: New York, 2006.
- (89) Konuk, R.; Cornelisse, J.; McGlyn, S. P. *J. Phys. Chem.* **1989**, 93, 7405–7408.
- (90) Bales, B. L.; Almgren, M. *J. Phys. Chem.* **1995**, 99, 15153–15162.